Preparation and characterisation of composite nanomaterials for radionuclide delivery

Pantalon Juraj, Natalija

Master's thesis / Diplomski rad

2016

Degree Grantor / Ustanova koja je dodijelila akademski / stručni stupanj: **University of Zagreb, Faculty of Chemical Engineering and Technology / Sveučilište u Zagrebu, Fakultet kemijskog inženjerstva i tehnologije**

Permanent link / Trajna poveznica: https://urn.nsk.hr/urn:nbn:hr:149:023711

Rights / Prava: In copyright/Zaštićeno autorskim pravom.

Download date / Datum preuzimanja: **2024-04-20**

Repository / Repozitorij:

Repository of Faculty of Chemical Engineering and Technology University of Zagreb

UNIVERSITY OF ZAGREB

FACULTY OF CHEMICAL ENGINEERING AND TECHNOLOGY

GRADUATE UNIVERSITY STUDY PROGRAMME

Natalija Pantalon Juraj

MASTER THESIS

Zagreb, July 2016.

UNIVERSITY OF ZAGREB

FACULTY OF CHEMICAL ENGINEERING AND TECHNOLOGY

GRADUATE UNIVERSITY STUDY PROGRAMME

Natalija Pantalon Juraj

PREPARATION AND CHARACTERISATION OF COMPOSITE NANOMATERIALS FOR RADIONUCLIDE DELIVERY

MASTER THESIS

Mentors:

Assistant Professor, Ján Kozempel, Ph.D.

Assistant Professor, Martin Vlk, Ph.D. (co-mentor)

Assistant Professor, Ivana Steinberg, Ph.D.

Examination committee members:

Assistant Professor, Ivana Steinberg, Ph.D.

Full Professor, Stanislav Kurajica, Ph.D.

Assistant Professor, Svjetlana Krištafor, Ph.D.

Zagreb, July 2016.

SVEUČILIŠTE U ZAGREBU
FAKULTET KEMIJSKOG INŽENJERSTVA I TEHNOLOGIJE
SVEUČILIŠNI DIPLOMSKI STUDIJ

Natalija Pantalon Juraj

PRIPREMA I KARAKTERIZACIJA KOMPOZITNIH NANOMATERIJALA ZA DOSTAVU RADIONUKLIDA

DIPLOMSKI RAD

Voditelji rada:

Doc. dr.sc. Ján Kozempel
Doc. dr.sc. Martin Vlk (ko-mentor)
Doc. dr. sc. Ivana Steinberg

Članovi ispitnog povjerenstva:

Doc. dr. sc. Ivana Steinberg
Prof. dr. sc. Stanislav Kurajica
Doc. dr. sc. Svjetlana Krištafor

Zagreb, srpanj 2016.

Summary

The aim of this thesis was to prepare composite nanomaterials for targeted delivery of radionuclides used for cancer diagnosis and therapy. Hydroxyapatite and TiO_2 nanoparticles were used as vehicles for targeted delivery because of their suitable properties such as biocompatibility and radiochemical stability. Nanocomposites were prepared by precipitating phosphonate ligands or polyethylene glycol with nanoparticles. The role of the phosphonates is binding of radionuclides and stabilisation of nanoparticles.

Prepared nanocomposites were labelled with ^{99m}Tc, a gamma emmiter used in tumor imaging and ^{223}Ra, an alpha emmiter used in targeted alpha therapy.

Phosphonic acids ethylenediamine tetra(methylenephosphonic) acid, propylenediamine tetra(methylenephosphonic) acid and 1,2-cyclohexyldiamine tetra(methylenephosphonic) acid were purified by ion exchange chromatography and used for preparation of nanocomposites. Besides mentioned ligands, methylene diphosphonic acid, etidronic acid, zoledronic acid, pamidronic acid and polyethylene glycol were used for experiments.

For labelling with ^{99m}Tc, the best yields were obtained for ^{99m}Tc-CDTMP-HAp (89%), and ^{99m}Tc-PDTMP-HAp (93%) stabilised before labelling and ^{99m}Tc-MDP-HAp (92%) and ^{99m}Tc-HEDP-HAp (89%) stabilised during their preparation. TiO_2 nanocomposites all had yields >93%.

Nanocomposites ^{223}Ra-zoledronic acid-HAp stabilised after labelling showed the best yields (60%) for labelling with ^{223}Ra.

Sažetak

Cilj ovog rada bio je priprema kompozitnih nanomaterijala za ciljanu dostavu radionuklida koji se koriste u dijagnostici i terapiji raka. Nanočestice hidroksiapatita i TiO_2 korištene su kao nosači za ciljanu dostavu zbog njihovih pogodnih svojstava, kao što su biokompatibilnost i radiokemijska stabilnost. Nanokompoziti su pripravljeni miješanjem fosfonatnih liganda ili polietilen glikola s nanočesticama. Uloga fosfonata je vezanje radionuklida i stabilizacija nanočestica.

Pripremljeni nanokompoziti obilježeni su s ^{99m}Tc, radionuklidom koji emitira gama zračenje i koristi se u dijagnostici tumora te ^{223}Ra, koji emitira alfa zračenje i koristi se u ciljanoj alfa terapiji.

Fosfonske kiseline, etilendiamin tetra(metilenfosfonska) kiselina, propilendiamin tetra(metilenfosfonska) kiselina i 1,2-cikloheksildiamin tetra(metilenfosfonska) kiselina, pročišćene su ionsko izmjenjivačkom kromatografijom i korištene su za pripravu nanokompozita. Osim navedenih liganda, u eksperimentima su korištene i metilen difosfonska, etidronska, zoledronska i pamidronska kiselina te polietilen glikol.

Za obilježavanje s ^{99m}Tc, najbolje iskorištenje dobiveno je za ^{99m}Tc-CDTMP-HAp (89%), i ^{99m}Tc-PDTMP-HAp (93%) stabilizirane prije označavanja i ^{99m}Tc-MDP-HAp (92%) i ^{99m}Tc-HEDP-HAp (89%) stabilizirane tijekom sinteze nanočestica. Svi nanokompoziti TiO_2 imali su iskorištenje veće od 93%.

Nanokompoziti ^{223}Ra-zoledronska kiselina-HAp stabilizirani nakon obilježavanja pokazali najbolje iskorištenje (60%) za označavanje s ^{223}Ra.

Ključne riječi: nanokompoziti, hidroksiapatit, TiO_2, fosfonske kiseline, ^{99m}Tc, ^{223}Ra

List of abbreviations

CDTMP   1,2- cyclohexyldiamine tetra(methylenephosphonic) acid

CT   computerised tomography

EDTMP   ethylenediamine tetra(methylenephosphonic) acid

EPR   enhanced permeability and retention effect

ESI   electrospray ionization

FT-IR   Fourier transform infrared spectroscopy

HAp   hydroxyapatite

HEDP   etidronic acid

IPA   isopropyl alcohol

LET   linear energy transfer

MDP   methylenediphosphonic acid

MEK   methyl ethyl ketone

MRI   magnetic resonance imaging

NMR   nuclear magnetic resonance

NP   nanoparticle

PDTMP   propylenediamine tetra(methylenephosphonic) acid

PEG   polyethylene glycol

PET   positron emission tomography

RES   reticuloendothelial system

RIT   radioimmunotherapy

RPS   radiopharmaceutical substances

SPECT   single-photon emission computed tomography

TAT   targeted alpha therapy

TBOT   tetra *n*-butyl orthotitanate

TNP   targeted nanoparticle

Contents

1. Introduction

Cancer has been one of the major social and health concerns for the last ten decades. The World Health Organization (WHO) reported that cancers are among the leading causes of morbidity and mortality worldwide, with approximately 14 million new cases and 8,2 million cancer related deaths in 2012. It is expected that annual cancer cases will rise from 14 million in 2012. to 22 within the next 2 decades [1].

Cancer exhibits up-regulated cell growth, with an ability for tumor cells to invade and metastasize. Conventional anticancer drugs exhibit a lack of specificity, poor solubility and distribution, unfavorable pharmacokinetics and high tissue damage or toxicity. Cancer nanotechnology is expected to transform current treatment systems by providing more efficient cancer diagnostics and therapeutics. Customized nanoscale constructs can serve as targeted drug delivery vehicles capable of delivering large doses of radionuclide or chemotherapeutic agents into malignant cells while sparing normal tissues, greatly reducing the side-effects that usually accompany many current cancer therapies.

The selection of potential radionuclides for tumor imaging and radionuclide radiotherapy involves the physical half-life, decay mode and the emission properties of the radionuclides. Gamma emitters with energy in the 150 keV range can be used for gamma imaging or single photon-emission tomography (SPECT), and high energy positron-emitters with energy of 511 keV can be applied for positron-emission tomography (PET). For targeted radionuclide radiotherapy applications, high and low energy β emitters are ideal radioisotopes for the treatment of small to large clusters of tumor cells. The tissue penetration range (1-10 mm), and cross fire effect of β particles can kill tumor cells in close proximity to neovasculature. Alpha-emitters hold great promise as therapeutics for small cancer lesions and micrometastatic cancers due to their high linear energy transfer (LET, 80 keV/μm) and short range energy depositions with tissue penetration range of 50-100 μm [2].

Generally, the characteristics of a radiometal that make it advantageous for use in the production of a radiopharmaceutical include a stable oxidation state, a well-defined coordination chemistry in aqueous environment, and relatively fast complexation kinetics at physiological pH [3].

Technetium-99m is so far the most commonly used radionuclide in nuclear imaging. This is due to its highly interesting physical properties such as short half-life (6 h) and gamma photon emission of 140 keV, which are advantageous for both effective imaging and patient safety perspectives. Alpha emitting radionuclide ^{223}Ra is suitable for use in radiotherapy of bone tumors and metastases due to its chemical similarity with Ca.

Radionuclides have to be delivered to the targeted tissue by suitable vehicles. Since no chemical bond can withstand high recoil energies of daughter atoms, advanced labelling and targeting strategies have to be employed. This research was focused on hydroxyapatite and TiO_2 nanoparticles stabilised with phosphonic acids which are the optimum compounds for delivering activity to bony tissues because of their high affinity for bone matrix hydroxyapatite.

2. Theoretical part

2.1. Nuclear medicine

Nuclear medicine was developed in the 1930s due to the discovery of naturally occurring radioactivity by Becquerel, the invention of the cyclotron by E.O. Lawrence and the development of the controlled-fission reactor. Studies with naturally occurring radioactive isotopes in plants and animals, such as the classic work of de Hevesy, followed shortly after. In the 1950s, ^{131}I was used to diagnose and treat thyroid cancer and disease. Soon afterwards, sodium iodine ($Na^{131}I$) became the first radiopharmaceutical approved in 1951. for clinical use by the United States Food and Drug Administration (FDA). Today, tens of millions of nuclear medicine procedures using radiopharmaceuticals are performed each year in more than 10,000 hospitals worldwide. The most common radionuclide used in diagnosis is ^{99m}Tc, accounting for 80% of all nuclear medicine procedures. Nowadays, the field of nuclear medicine is evolving from anatomic toward molecular medicine, focusing more on the cellular and molecular pathways and mechanisms of disease [4].

The diagnosis and treatment of many tumors stills remains elusive and a major barrier to effective clinical outcomes. Cancer cells are known to possess unique characteristics of dividing and proliferating rapidly, resisting cell death or apoptosis and having devastating invasive potentials. Also, tumor cells have the ability to infiltrate surrounding normal tissues or penetrate into lymphatics and/or blood vessels enabling them to circulate and migrate to multiple distant sites or organs, forming secondary tumors.

Most conventional treatments for management of cancers involve chemotherapy using low molecular weight anticancer agents that are systemically administered by the intravenous (i.v.) route. This intervention inherently lacks the ability to target tumors selectively.

Low molecular weight anticancer compounds also suffer from short plasma circulation half-lives due to their rapid clearance through renal excretion. Also naked proteins, peptides, DNA, small interfering RNA (siRNA), and therapeutic molecules that are administered via the blood stream are generally labile and prone to degradation in the presence of serum or plasma components [5].

Nuclear medicine plays crucial role in the modern approach to cancer treatment by providing means to the following:

- Determine the extent or severity of the disease, including metastases
- Select the most effective therapy based on the unique biological characteristics of the patient and the molecular properties of a tumor

- Accurately assess the effectiveness of a treatment regimen
- Adapt treatment plans quickly in response to changes in molecular and biochemical characteristics of the tumor
- Assess disease progression
- Identify recurrence of disease and help manage ongoing care [6]

2.1.1. Nuclear imaging methods

Diagnostic (or contrast) agents enhance visibility of specific tissues by increasing the signal to noise ratio relative to surrounding tissues and are generally optimized to provide a quick, high-fidelity snapshot of the living system. Molecular imaging modalities (Fig.1) include MRI, CT, US, optical imaging (bioluminescence and fluorescence), single photon emission computed tomography (SPECT) and positron emission tomography (PET) [7].
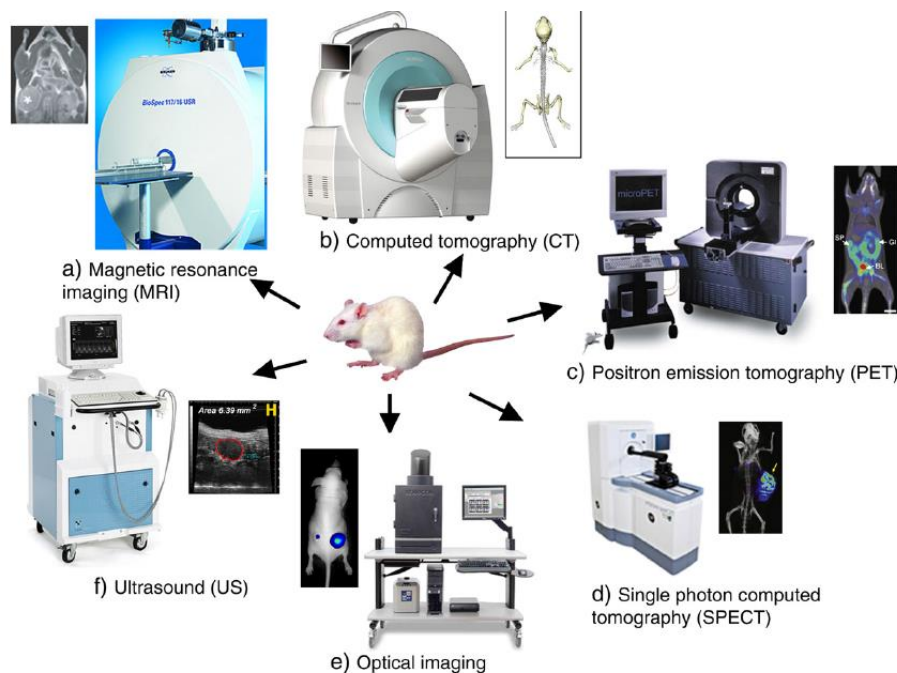
Figure 1. Typical molecular imaging instruments and images representative of each modality [7].

SPECT forms a three-dimensional image of the distribution of gamma-emitting radiotracers injected into the body. One advantage of SPECT is that multiple probes labelled with separate

isotopes may be studied in parallel since each isotope might be associated with its unique γ spectrum [6].

PET, similar to SPECT, provides information about biochemical and physiological processes in the human body. For PET applications, positron-emitting radionuclides of first choice are ^{18}F, ^{11}C, ^{13}N, and [15]O. These elements are able to emit a positive electron from the nucleus. This positive electron, in turn, travels only a short distance through the tissue and interacts with a free or loosely bound negative electron. The outcome of this interaction is one positive electron and one negative electron annihilating each other, with the masses beeing converted into two photons, each consisting of 511 keV of energy and beeing given off in opposite directions (Fig.2).
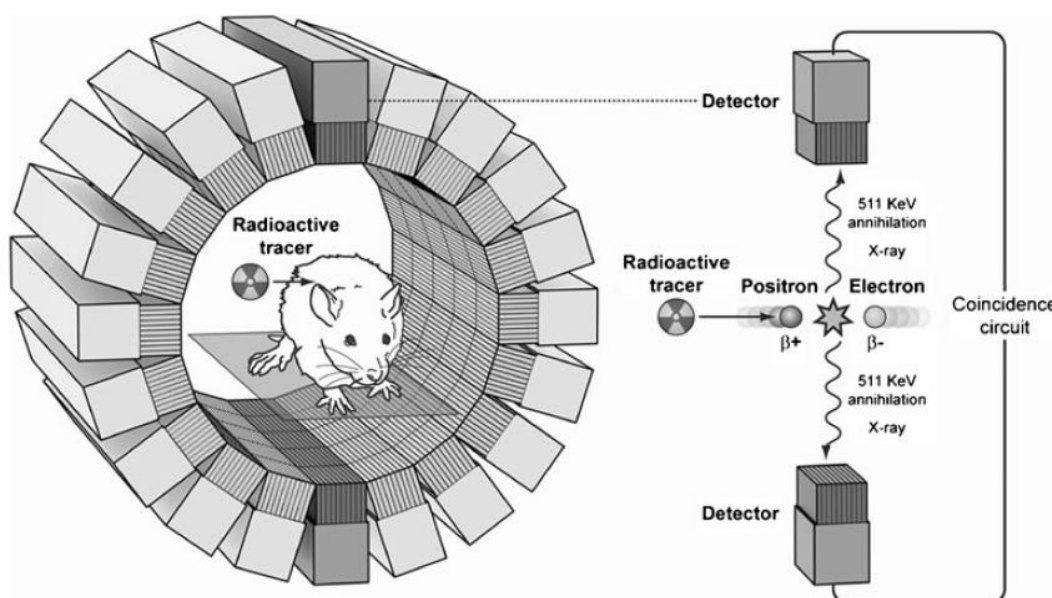
Figure 2. A schematic diagram showing positron emission during the decay process of a radionuclide [6].

The principal applied radionuclide for PET is Fluor-18 (^{18}F) which is known for its ideal half-life to manage (1,83 h). The development of the radiopharmaceutical [2-^{18}F]-2-fluoro-2-deoxyglucose ([18]FDG) has been so far an important progress for PET imaging in oncology. [18]FDG acts as a glucose analogue allowing the visualization of glucose consumption, a metabolic process being massively enhanced in many malignancies [8].

2.1.2. Radionuclide therapy

Radiopharmaceuticals are dosage forms consisting of one or two components, a carrier, a trace amount of radionuclide with a defined radiation type, or their combination. Therefore, the efficacy of a radiopharmaceutical is determined by its components. In tumor radiotherapy, the therapeutic effect is due to the tumoral absorption of alpha (α) or beta (β) radiation energy emitted by the radionuclide. The ideal radiopharmaceutical should convey the radioactive nuclide quantitatively to the tumor tissue, with no radiation reaching the normal tissues [2].

Table 1. Characteristics of potential radionuclides for nanotargeted tumor imaging [2].

Radionuclide	Emission type	Half-life	E_{max} (γ), (keV)
^{131}I	γ (81,2%), β	8,0 days	284, 364, 637
^{67}Ga	γ	78,3 h	93, 184, 300, 393
^{111}In	Auger, γ	67,2 h	171, 245
^{123}I	Auger, γ	13,2 h	159
^{99m}Tc	γ	6,0 h	140
^{18}F	Positron	1,83 h	511
^{64}Cu	Positron	12,7 h	511

Table 2. Characteristics of potential radionuclides for tumor radiotherapy [2].

Radionuclide	Emission type	Half-life	E_{max} (MeV)	R_{max} (mean)[1]	Size of tumor cells[2]
^{186}Re	β, γ (9,4%)	89,2 h	1,07	5 mm (0,9 mm)	Intermediate clusters
^{188}Re	β, γ (15,1%)	17 h	2,12	11 mm (2,4 mm)	Large clusters
^{177}Lu	β	161 h	0,49	1,6 mm (0,67 mm)	Small clusters
^{131}I	γ (81,2%)	8 d	0,28; 0,36; 0,64	2,0 mm	Small clusters
^{90}Y	β	64,1 h	2,28	12 mm (2,8 mm)	Large clusters
^{67}Cu	β	2,6 d	0,19	0,7 mm	Small clusters
^{225}Ac	α	10 d	5,83; 5,79; 5,79; 5,73	40-80 μm	Single cells and small clusters
^{211}At	α	7,2 h	5,87	60-80 μm	Single cells and small clusters
^{111}In	Auger, γ	67 h	0,42	2-500 nm	Single cells

[1]Radiation tumor tissue penetration maximum and mean range. [2]Small, intermediate and large clusters correspond approximately to the intervals 10^6, 10^6-10^8, and 10^8-10^{10} tumor cells per cluster, respecitevely.

The choice of radionuclide depends on its particular application. While radionuclides used for nuclear medicine imaging (Table 1) emit gamma rays, which can penetrate deeply into the body, radionuclides used for therapy (Table 2) must emit radiation with a relatively short path length in order to deposit their energy locally and minimize the whole-body irradiation. There

are three types of particulate radiation of consequence for radionuclide therapy: beta particles, alpha particles, and Auger electrons [6].

The major criteria for diagnostic use of radioisotopes are:

- suitable physical properties, i.e. a high detection efficiency for the radionuclide, compatible with the lowest possible radiation dose to the patient
- suitable biochemical properties, especially organ selectivity and comptability with the bio-kinetics.

As far as physical properties are concerned, the half-life should be short (between a few minutes and a few hours) and the decay should occur preferably via IT, EC or β^+ emission. Furthermore, the specific radioactivity of the final product should be rather high. In general, the diagnostic radioisotopes are classified into two groups, namely γ emitters (e.g. ^{67}Ga, ^{111}In, ^{201}Tl, etc.) and β^+ emitters (e.g. ^{15}O, ^{18}F, etc.). If the radioisotope emits a single γ ray, SPECT can be used; in the case of β^+ emitters, PET is very advantageous. Because of its quantitative nature, rapidity and higher resolution, PET is superior to SPECT [9].

One of the main pharmacological characteristics of diagnostic RPS (radiopharmaceutical substances) is the high ratio of activity accumulated per g of tumor to the activity taken up per g of soft tissue (the differential accumulation level). The blood elimination time must be short for high values of the ratio to be obtained, and the rate of accumulation of RPS in the lesion site must be maximal. On the other hand, the retention time of the labelled agent in blood should be optimal for reaching the receptor sites of tumors and the greatest level of accumulation in affected tissue. Furthermore, the RPS must be rapidly excreted from the body with urine to avoid accumulation in the gastrointestinal tract. This is of particular importance for therapeutic RPS, as excretion via the hepatobiliary system often leads to radionuclide accumulation in the gastrointestinal tract, leading to increased dose loads on the abdominal organs [10].

Biological targeting molecules of radiopharmaceuticals range from antibodies to antibody fragments, proteins, peptides and nucleic acids. More recently, a new type of molecules, namely nanoparticles or nanocarriers, has entered the radiopharmaceuticals area. Target specific nanoparticle radiopharmaceuticals can have a higher number of targeting molecules and radionuclides per particle [4]. Nanoparticles based on lipid- and polymer-formulations are developed as potential drug delivery agents [11], for example copolymers of N-isopropylmethacrylamide [12] which hydrophobically entrapped the therapeutic

radionuclide, [64]Cu. Another approach for targeted delivery of radionuclides is using magnetic forces to target and hold magnetic nanoparticles in vivo at anatomical sites with restricted access [13, 14].

2.1.2.1. *Radioimmunotherapy*

Radioimmunotherapy (RIT) combines the advantages of radiation therapy and specific immunotherapy using mAbs. The antibody serves primarily as a delivery vehicle of radiation and has no significant effect on the function. The therapeutic effect is achieved by tissue absorption of the energies from continuous, low-dose radiation emitted from the radionuclides tagged to mAbs.

The exact choice of radionuclide used for RIT depends on the radiation characteristics of the nuclide, the radiolabeling chemistry, and the type of malignancy or cells targeted. Beta emitters, because of their lower energy and longer path length, are more suitable for targeting bulky, solid tumors, whereas alpha emitters and Auger emitters, with their high LET and short-distance energy deposition, are better suited for targeting single cells, as in micrometastatic disease, blood borne malignancies, and locoregional applications [6]. The range of different emitters is shown in Figure 3.
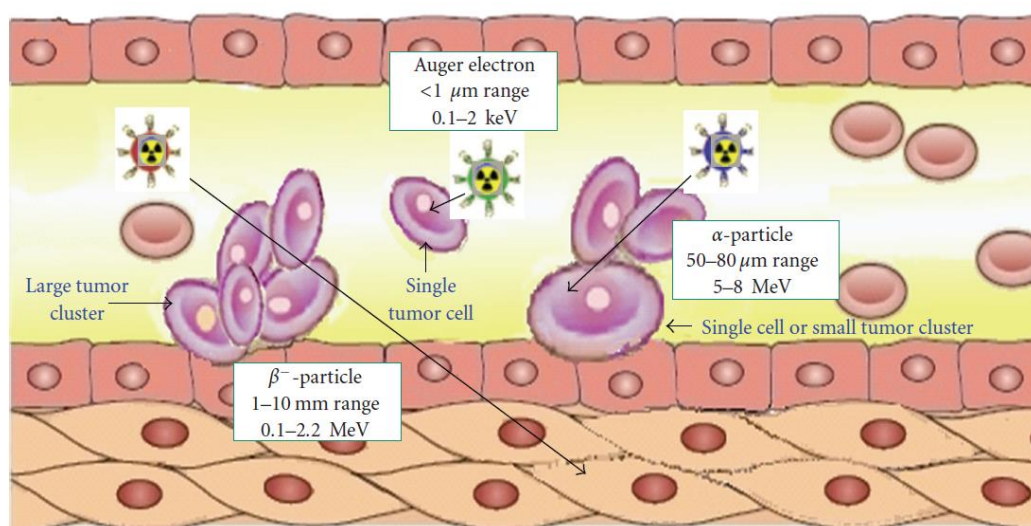
Figure 3. Schematic diagram of tumor tissue penetration range of internal radiotherapy by Auger electron (0,1–2 keV, <1 μm), α (5–8MeV, 50–80 μm range), and β- (0,1–2,2MeV, 1-10 mm range) radiation emitters [2].

2.1.2.2.   *TAT targeted alpha particle therapy*

The effectiveness of targeted alpha therapy (TAT) can be explained by the properties of α particles. Alpha particles are helium nuclei ~8,000 times larger than β⁻ particles (electrons). When emitted from radionuclides that decay via an α decay pathway, they release enormous amounts of energy over a very short distance. Typically, the range of α particles in tissue is 50–100 μm and they have high linear energy transfer (LET) with a mean energy deposition of 100 keV/μm, providing a more specific tumor cell killing ability without damage to the surrounding normal tissues than β⁻ emitters (Fig.4).
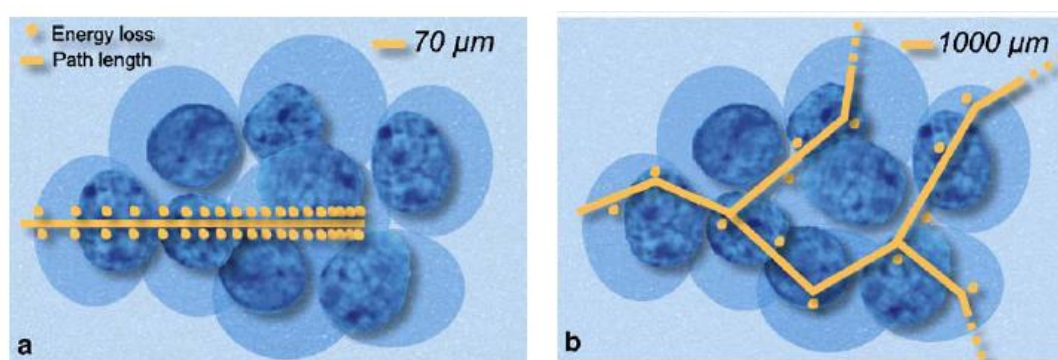
Figure 4. (a) Short path length of α particles, in the range of a few cell diameters, compared with (b) the longer path length of β particles [15].

Importantly, this high linear energy transfer (high-LET) radiation is not dependent on active cell proliferation or oxygenation, and the resulting DNA damage caused by α-particles is much more difficult to repair than that of β⁻. Radiation induces single- and doublestranded DNA break, causes apoptosis, and initiates overexpression of p53, leading to delays in the G1 phase of the cell cycle. Death of cells exposed to α-particles occurs only when the particles traverse the nucleus; high concentrations of α-particles directed at the cytoplasm have no effect on cell proliferation [16].

Due to these properties, the majority of pre-clinical and clinical trials have demonstrated that α emitters such as ^{225}Ac, ^{211}At, ^{212}Bi, ^{213}Bi, ^{212}Pb, ^{223}Ra, and ^{227}Th are ideal for treatment of smaller tumor burdens, micrometastatic disease, and disseminated disease.

Even though these α emitters have favorable properties, the development of TAT has been limited by high costs, unresolved chemistry, and limited availability of the radionuclides. To overcome these limitations, more potent isotopes, additional sources, and more efficient isotope production methods should be addressed. Furthermore, better chelation and labelling

methods with improvements of isotope delivery, targeting vehicles, molecular targets, and identification of appropriate clinical applications are still required [17, 18].Bone metastasis cause severe pain, so there have been many attempts to develop curative treatment regimens. Beta emitting radiopharmaceuticals for bone targeting, such as ^{89}Sr chloride, have been used clinically for treatment of bone pain. Although β emitters relieve bone pain associated with metastatic lesions in the skeleton, bone marrow toxicity limits use of high dose radiations to prevent tumor progression due to the long radiation range of β particles. To overcome this drawback, clinical use of several low energy α emitters, including [153]Sm and [186]Re, and the conversion electron emitter [117m]Sn, have been examined. Among these radionuclides, [153]Sm complexed with ethylenediamine tetra(methylenephosphonic) acid (EDTMP), has been approved for use in palliation of bone pain by the U.S. FDA. Reduction of bone marrow exposure can be achieved due to the short range of α particles. A comparative study using bisphosphonates labelled with α emitting [211]At and β emitting ^{131}I indicated that the bone surface-to-bone marrow ratio was threefold higher with [211]At than with [131]I [19].

Bismuth-213, an α emitter with a half-life of 46 min, has shown to be effective in preclinical as well as in clinical applications, for example, glioma therapy [20] and treatment of larger neuroendocrine tumours with [213]Bi-DOTATATE [21].

Another point to be considered when the two forms of RIT (α and β) are compared is the dosimetry. The variation of α particle energy loss in matter is stochastic, necessitating the use of specific microdosimetric methods such as Monte Carlo calculation or analytical methods. These methods make it possible to calculate probability densities of specific energy (energy deposited in the targeted cellular volume and more often the cell nucleus), equivalent to the absorbed dose [15].

2.2.   Targeted drug delivery

Radiolabelled nanocarriers can be designed and used for cancer diagnostic and therapeutic purposes when tagged with appropriate radionuclides. Conventional anticancer drugs exhibit a lack of specificity, poor solubility and distribution, unfavorable pharmacokinetics and high tissue damage or toxicity. Targeted drug delivery systems such as passive and active targeting nanocarriers (Fig.5), with diameters ranging from 10-100 nm have been developed to improve the biodistribution, pharmacological, therapeutic and toxicity properties of agents used in

cancer diagnostics and therapeutics. One of the major challenges is to design a nanocarrier with less immunotoxic effect and to avoid biological barriers in the body such as to reduce delivered diagnostic and therapeutic agent uptake in the reticuloendothelial system (RES) [2].
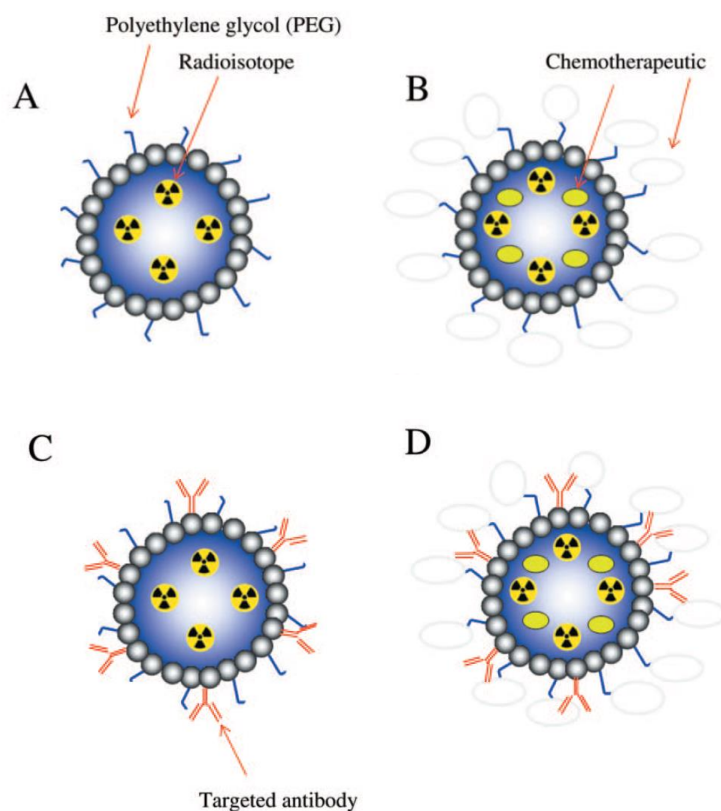
Figure 5. Schematic representation of passive (A, B) and active (C, D) targeting nanoliposome encapsulated with radionuclides (A, C) and co-delivery of radiochemotherapeutics (B, D) [2].

As a platform, nanoparticles are wellsuited for developing targeted contrast agents, because:

- they have a surface, which can be functionalized with one or more targeting molecules at a wide range of densities;
- their plasma circulation time can be tuned over several orders of magnitude based on their physico-chemical properties;
- contrast agents and drugs can be included at predetermined ratios either in the interior or on the surface.

Nanoparticles can be made from a number of materials including proteins, peptides, polymers, lipids, metals and metal oxides, and carbon. The most relevant nanoparticle structures include

drug conjugates and complexes, dendrimers, vesicles, micelles, core–shell structures, microbubbles, and carbon nanotubes, which can all be functionalized with a targeting moiety, therapeutic, and contrast agent [7].

2.2.1. Radiolabelled nanocarriers

Current progress in nanomedicine has exploited the possibility of designing tumor-targeted nanocarriers being able to deliver radionuclide payloads in a site or molecular selective manner to improve the efficacy and safety of cancer imaging and therapy. Radionuclides of auger electron, α, β, and γ radiation emitters have been surface-bioconjugated or after-loaded in nanoparticles to improve the efficacy and reduce the toxicity of cancer imaging and therapy in preclinical and clinical studies [2].

An ideal TNP (targeted nanoparticle) may have molecular targeting that can be imaged during its circulation in the body. Upon reaching its destination, it may have targeting moieties that associate with cellsurface receptors, internalize into the cytosol, target the intracellular target if necessary, and release the active therapeutic [7].

There are five approaches generally used for labelling or encapsulating radionuclides on nanocarriers:

- Labelling nanocarriers by encapsulation during preparation;
- nanocarrier surface labelling after preparation;
- nanocarrier surface labelling of bioconjugates after preparation;
- incorporation into the lipid bilayer after preparation;
- after-loading of the aqueous phase of the nanocarriers after preparation. [2]

There are three generations of nanocarriers developed: (i) the first generation of nanocarriers (passive targeting) which are rapidly trapped in the reticuloendothelial system (RES) organs (e.g., liver and/or spleen), (ii) the second generation of sterically stabilised PEGylated nanocarriers (passive targeting), which can evade the RES of the liver and spleen, enjoys a prolonged circulation in the blood and allows for passive targeting through the enhanced permeability and retention (EPR) effect in leaky tumor tissues, and (iii) the third generation of nanocarriers with a bioconjugated surface modification of the nanoparticles using specific

antibodies or peptides to actively target specific tumors or tissues through molecular interaction or affinity (active targeting).

The main disadvantage of radionuclides is that no chelator or other type of labelled molecule can withhold the recoil energy of daughter hot atoms generated in such decays. Every hot daughter atom is thus immediately released from the carrier molecule and may cause severe damage to healthy tissues in vivo, particularly when applied systemically. Some nano-size engineered constructs are at least partially able to retain recoiled atoms and ensure proper therapeutical dose targeting due to their physical and chemical properties [22].

The selection of a proper radionuclide system may partially eliminate the problem of recoils release, when very short half-life values of daughter nuclei in a cascade (ns - μs - s) do not allow significant spread of activity from the location of the mother nuclide. The drawback of recoils release however leads to advanced design of novel radionuclide carriers based on nanomaterials.

Released kinetic energy in the decay is distributed among the decay products following their masses according to the law of momentum conservation. Recoil energy released in the alpha particle decay can be in raw estimation expressed by the approximate relation (1):

$$E_r = E_\alpha \ \frac{m_\alpha}{M_X} \hspace{3cm} (1)$$

Where the E_r is the recoil energy of a daughter atom, E_α the energy of released alpha particle, m_α is the rest mass of emitted alpha particle, and M_X is mass of the daughter hot atom. Part of the recoil energy may be converted to translational energy of the remaining molecule or consumed for its dissociation. Chemical bond strength ranges typically in the order of magnitude of 1-10 eV, while kinetic energy of daughter hot atom usually reaches ≈ 100 keV in case of alpha particle decays. This is several orders of magnitude higher, compared to the energy of any chemical bond. On the other hand, to stabilise such hot atom in a molecular structure, to completely loose its energy (e.g. by inelastic scattering, ionization, excitation, etc.), it must hit several thousands of chemical bonds in e.g. a crystallite structure or in a polymer.

Another important parameter is the recoils charge that may cause additional damage via electronic interaction with the nanoconstructs. For example, the recoils of ^{223}Ra produced in ^{227}Th decay reach the charge values of up to 40^+. These supercharged hot atoms finally neutralize via interactions with their surroundings, while they ionize and excite molecules

along their path and release most of their energy at the end of their path, around the Bragg peak.

The elimination of recoils release from nanoconstructs *in vivo* could be generally achieved by three approaches. Firstly, the recoil energy is gradually attenuated in the intrinsic nanoconstruct material ("stopping by size"). Secondly, the final stabilisation of thermalized hot atom is achieved in a depot of multiple functional groups surrounding its track carried by several thousands of nanoconstructs ("stopping by depot"). In this case, the hot atom originating from one nanoconstruct after passing several other nanoconstruct units loses its energy and is finally stabilised in another nanoconstruct of the depot. To promote the trapping ability, the surface of the nanoconstruct is typically covered by many functionalities capable of catching such atom (e.g. functional groups, structural cavities, etc.). Finally, the third approach is performed only by the selection of a radionuclide system with appropriate decay parameters ("stopping by time"). All the approaches mentioned can be combined together, so the overall release of daughter recoils is almost insignificant. Another highly important issue is proper targeting of the nanocontructs. It could be achieved similarly as for multimodal constructs used mainly for imaging. The elimination of the uptake of nanoconstructs in RES could be achieved by proper surface coating and advanced drug-delivery systems [22].

2.2.2. *Labelling of nanoparticles*

A very powerful and sensitive method to determine the *in vivo* behavior of NPs relies on radiolabelling and subsequent detection with single photon emission computed tomography (SPECT) or positron emission tomography (PET). Radiolabelling of NPs follows essentially two strategies; an "extrinsic" one in which potent, NP surface-bound chelators such as 1,4,7,10-tetraazacyclododecane-1,4,7,10-tetraacetic acid (DOTA) or 1,4,7-triazacyclononane-1,4,7-triacetic acid (NOTA), are directly labelled with ^{64}Cu or ^{68}Ga. Alternatively, complexes with bifunctional chelators are subsequently coated to the NP surface. In the "intrinsic" approach, the radiolabel is an integral part of the NP and no additional chelators are required [23].

In many cases, proton irradiation of nanoparticles allows radiolabelling by transmutation of a tiny fraction of their constituent atoms into radionuclides. However, not all types of nanoparticles offer nuclear reactions leading to radionuclides with adequate radiotracer properties [24].

There are approximately 100 α emitting radionuclides (essentially heavy isotopes with an atomic number ≥82), but only a small number of them are available for clinical use. The majority of these α emitting radionuclides are produced in nuclear reactors; only a few are cyclotron products. In the case of radionuclides with a short physical half-life (such as bismuth-213), the duration of elution and compound purification must be short enough to obtain a radiopharmaceutical of good radiochemical quality and purity. The selection of α emitting radionuclides also has to take into account daughter products which could be metabolised in a different way than the parent [15].

An example of radionuclide production is the separation of ^{99}Mo from ^{235}UAl$_3$ -alloy. The chemically separated ^{99}Mo is used to prepare a generator system. This consists of loading the ^{99}Mo activity on an Al$_2$O$_3$ column and milking off the decay product ^{99m}Tc periodically by elution with saline. The ^{99}Mo/^{99m}Tc generator is the most commonly used system in diagnostic nuclear medicine. Due to the ideal imaging properties of ^{99m}Tc with SPECT, about 80% of all nuclear medical procedures are performed worldwide with it. The generator form makes the availability of ^{99m}Tc easy; its specific radioactivity is very high. The product is used directly for labelling biomolecules [9].

Alpha emitting radionuclides ^{224}Ra and ^{223}Ra are the most suitable radium isotopes for use in radiotherapy of bone tumors and metastases owing to their chemical similarity with Ca. Radium-224 is used as a starting radionuclide in generators for production and medicobiological studies of ^{212}Pb/^{212}Bi, and also for treatment of Bechterew's disease and skeletal tuberculosis. The main drawback of using ^{224}Ra in nuclear medicine is production of a relatively long-lived gaseous daughter radionuclide, ^{220}Rn ($T_{1/2}$=55,6 s), and, as a consequence, possible redistribution of the decay products in a living body. Furthermore, in the radioactive decay chain of ^{224}Ra, there is ^{208}Tl (3,1 min) emitting hard (2,6 MeV) γ radiation.

The use of ^{223}Ra in nuclear medicine is preferable compared to ^{224}Ra because the daughter radionuclide of ^{223}Ra, gaseous ^{219}Rn (3,9 s), has a shorter half-life, so the decay products are mainly localized in the vicinity of the parent radionuclide. The total energy of α particles emitted in the course of the decay of ^{223}Ra and its daughter products is ~27 MeV. Relatively long halflife of ^{223}Ra (11,4 days) allows centralized production of radiopharmaceuticals and their delivery to various institutions remote from the production site.

The first radiopharmaceutical, Alpharadin, based on $^{223}RaCl_2$, passed preclinical and clinical tests and in 2013. it was approved by the FDA (US Food and Drug Administration) for clinical use in the form of Xofigo commercial product.

There are several types of radioisotope generators for production of short-lived α emitters and their separation from parent radionuclides, differing in the separation method used: ion exchange, extraction, distillation, etc. Today, ion-exchange and extraction-chromatographic generators seem to be the most efficient and the safest because of their simple design, radiation safety, possibility of automating the separation of highly radioactive elements, and convenience of transportation. The parent radionuclide in such generators is sorbed and firmly retained on a chromatographic column packed with an appropriate sorbent, and the short-lived daughter radionuclide is eluted in the batch or continuous mode (depending on the half-life) with an appropriate eluent.

For production of ^{223}Ra, extraction-chromatographic $^{227}Ac/^{223}Ra$ generator, ion-exchange $^{227}Ac/^{227}Th/^{223}Ra$ generator and extraction $^{227}Ac/^{223}Ra$ generator can be used [25].

2.3.   Components of composite nanomaterials

Nanomaterials have recently been envisioned as carriers for radioisotopes in targeted radioimmunotherapy (RIT), targeted alpha therapy (TAT), and medical diagnostic imaging. This approach aims to overcome the global radiotoxicity of parent radionuclides and associated daughters, one of the main limitations of TAT. Inorganic nanomaterials are of interest as carriers because of their characteristic size-shape dependent properties, stable crystalline structures, and functionalizable surfaces [26].

The ideal attributes of microspheres or particulates for use as carriers of radionuclides for intra-arterial therapy are biocompatibility, biodegradability, ease of radiolabelling and high radiochemical stability of the labelled products to resist the possible leaching of radionuclide *in vivo* [27].

2.3.1. *Titanium dioxide*

Titanium dioxide (TiO_2) has a great number of applications due to its strong oxidizing power of the photogenerated holes, chemical inertness, non-toxicity, low cost, high refractive index and other advantageous surface properties. It is used in as a white pigment in paints, plastics,

paper and cosmetic products which represent the major end-use sectors of TiO_2 [28]. Nanoparticulate TiO_2, one of the most prevalent nanoparticle types, is produced in large-scale industrial processes for a wide range of applications.

A recent study [29] presents three different options for radiolabelling of commercial TiO_2 nanoparticles for particle detection, localization, and tracing under various experimental conditions. The limits for detection of TiO_2 nanoparticles in concentrations as low as 0,5 ng/L could be realized in complex systems without the necessity of intense sample purification or pretreatment.

2.3.2. Hydroxyapatite

Hydroxyapatite ($Ca_{10}(PO_4)_6(OH)_2$, HAp) is a major mineral component in animals and humans and is widely studied due to its excellent biocompatibility, bioactivity and similarity in chemical composition with human bone tissues. As such, it is utilized in many biomedical applications such as orthopaedic implants, sustained drug release systems and as an adsorbent in column chromatography for purification and separation of nucleic acids and proteins [30]. A wide range of applications for HAp is possible because its properties can be tailored by controlling its composition, for example by substitution in the crystal structure, particle size and morphology prior to usage.
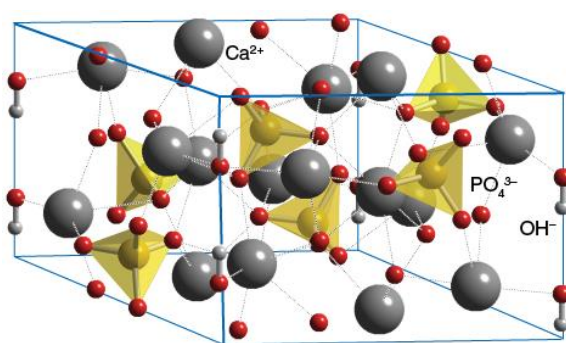
Figure 6. Hydroxyapatite crystal structure.

HAp particles get converted to Ca^{2+} and PO_4^{3-} ions by natural metabolic process and eliminated over a period of 6 weeks, thereby ensuring excellent biocompatibility. Moreover, HAp particles can be easily tagged with lanthanide radioisotopes, resulting in highly stable radiolabelled preparations owing to the high chemical affinity of PO_4^{3-} for the Ln^{3+} ions [27].

Radioisotopes can be conjugated to HAp crystals using various linkers and chemical modifications of the particle surfaces. In 2007., Ong [31] reported that HAp nanoparticles can easily and rapidly (within 15 min) be loaded with drugs or radioisotopes by exploiting the high-affinity interaction between HAp and polyphosphonates. There are two main reasons for exploiting this interaction for drug or isotope loading on the HApNPs. First, it eliminates the need for surface chemical modifications of the HApNPs and second, various phosphonates are already used routinely in the clinic for treatment of a variety of diseases or as imaging agents [31].

2.3.3. *Phosphonic acids*

Metastatic lesions of bones are among the most common complications of solid tumors such as breast, prostate, and lung tumors. Bone metastases in most of these patients lead to the development of a number of complications: bone pain, pathological fractures, and hypercalcemia, resulting in an overall deterioration in patients' quality of life.

Phosphonic acids and their salts are optimum compounds for delivering activity to bony tissues. This is a class of drugs, created on the basis of inorganic pyrophosphates in which the oxygen atom in the pyrophosphate molecule (P-O-P) is substituted with a carbon atom (P-C-P). While pyrophosphate is subject to hydrolysis by phosphatases, phosphonates are enzyme-resistant. These agents have affinity for bone matrix hydroxyapatite and show selective accumulation in zones with increased mineralization requirements, especially in metastatic and inflammatory-destructive foci.

Phosphonates can have direct effects on tumor cells, stimulating apoptosis, inhibiting angiogenesis and matrix metalloproteases, decreasing tumor cell adhesion, and decreasing vascular endothelial growth factor levels. Multidentate polyaminophosphonic acids are widely used to create stable complex compounds with a variety of radionuclides, including lanthanoids. Among these are ethylenediamine tetra(methylenephosphonic) acid (EDTMP), 1,4,7,10-tetraazacyclododecane-1,4,7,10-tetra(methylenephosphonic) acid (DOTMP), propylenediamine tetra(methylenephosphonic) acid (PDTMP), diethylenetriaminopentakis-(methylphosphonic) acid (PPA), and others. Lexidronam, (^{153}Sm-EDTMP) has undergone clinical trials and has been approved for clinical use. Depending on the use of the agent, radioactive labels are radionuclides such as ^{99m}Tc, ^{68}Ga, ^{153}Sm, ^{166}Ho, ^{188}Re, ^{177}Lu, ^{170}Tm, ^{90}Y, ^{227}Th, ^{228}Ac, ^{212}Bi, and others. Technetium-99m is widely used in radionuclide diagnosis,

because of its unique nuclear physics and chemical properties. ^{99m}Tc has an optimum halflife (6 h) and γ quantum energy (140 keV).

Gallium-68 is a potential radionuclide for creating radiopharmaceuticals for diagnosis of metastatic bone lesions by positron emission tomography (PET) using phosphonates as carrier molecules. The isotope ^{68}Ga has optimum nuclear physics properties ($T_{1/2} = 68$ min, $\beta^+ = 89\%$, $E^+_{\beta\ max} = 1.9$ MeV). A great advantage of ^{68}Ga is that it can be prepared using a commercially available ^{68}Ge/^{68}Ga generator.

The selective accumulation of radionuclides in bony tissue is explained by the following mechanisms of adsorption of diphosphonates labelled with radioactive isotopes by hydroxyapatites [($Ca_{10}(PO_4)_6(OH)_2$]:

- Adsorption of alkali-substituted elements (for example, ^{89}Sr(II)) by exchange for calcium ions in bone tissue;
- Interaction of charged three- and four-valent cations with hydroxyapatites to form insoluble phosphates or hydroxides, which attach tightly to the mineral components of bone tissue. This mechanism applies to the adsorption of ^{153}Sm(III), ^{166}Ho(III), and ^{117m}Sn(III), forming thermodynamically stable structures with minimal resorption of bone in *in vivo* conditions;
- Chemosorption of phosphates and diphosphonates onto the hydroxyapatite surface. Examples include ^{32}P-orthophosphate and organophosphate compounds labelled with ^{32}P, ^{131}I, and ^{211}At;
- Formation of bridging groups between ions of the radioactive metal and hydroxyapatite in the presence of multidentate phosphonate and carboxyl chelate complexes. By this mechanism, ^{186}Re and ^{188}Re-HEDP are sorbed.

The location of phosphonate complexes in bone is explained by the chemical affinities of diphosphonic acids for calcium in growing bone tissue. It has been suggested that tetraphosphonates may have greater chemical affinity for bone tissue. Multidentate aminophosphate ligands form more stable chelate complexes than diphosphonate ligands [10].

Figure 7. Tetraphosphonic acids: 1,4,7,10-tetraazacyclododecyl tetraaminotetramethylenephosphonic acid (a), dimethylpropylenediamine tetra(methylenephosphonic) acid (b).

In literature, a stable complex with technetium-99m has been prepared using a multidentate phosphonate ligand Am-Bz-EDTMP (aminobenzyl ethylenediamine tetra(methyl phosphonic) acid). This complex showed best high bone uptake, low non -osseous uptake, and rapid blood clearance, which warranted its further investigation [32].

Figure 8. Aminobenzyl ethylenediamine tetra(methylphosphonic) acid (Am-Bz-EDTMP).

3. Experimental part

3.1.   General procedure

Samples were measured on FT-IR spectrometer iS50, reflection ATR technique on diamond crystals. Spectra were measured in the mid-IR spectral region (MIR) from 4000 to 400 cm^{-1} with a resolution of 2 cm^{-1}, and further evaluated in the program Omnic 9.1.

The NMR spectra were recorded on Bruker Avance II 300 (^{1}H at 300,13 MHz and ^{13}C at 75,45 MHz) in solution ^2H_2O. For ^{1}H NMR, dioxane was used as an internal standard. Chemical shifts of ^{13}C NMR spectra were referenced relative to δ (dioxane) = 66,66 ppm. ESI mass spectra were recorded on Finnigan MAT SSQ 7000 in MeOH. The purity of the samples was monitored by TLC foils Kieselgel 60 F_{254} (Merck). Detection of the TLC sheet was performed by means of UV light (Model UVS 54, 254 nm). Products were dried on a vacuum line with the internal branch of a low-temperature cooler connected via a rotary oil pump LAVAT VRO 04/21 classic, bicameral pump. Other instruments were a centrifuge MPW Med Instruments, Model MPW-350, vibrational mixer VELP Scientific (P-LAB Inc.), a magnetic stirrer used with heating and IKAMAG rotavapor BUCHI R-215. Ultrapure water was prepared by apparatus Direct-Q3, water purification system MILLIPORE. For dispersion of samples, Branson Digital Sonifier and Elmasonic S 100 H ultrasonic bath were used.

Activities of reaction mixtures were measured on a radioactivity detector with ionization chamber type CII CRC 55tW (CAPINTEC), a well type NaI(Tl) detector. The yields of labelled acids were determined by paper chromatography on Whatman 1 paper, by measuring the activity on Bioscan AR-2000 Radio-TLC Imaging Scanner (Canberra Packard) with P10 (argone-methane mixture) counting gas (Linde).

Samples were filtered through PTFE (13 mm, 0,22 μm) syringe filters.

3.1.1. Used chemicals

In experiments, the following chemicals were used: methylenediphosphonic acid, etidronic acid and 95% pamidronate disodium salt hydrate (Sigma Aldrich), zoledronic acid (solution for infusion, Sandoz), concentrated HCl 37% p.a., isopropanol p.a., citric acid and ammonium hydroxide 25% p.a. from Lachner, tetrabutyl ortho titanate p.a. (Merck), $SnCl_2 \cdot 2H_2O$ from BDH LTD, NaCl (Chemapol), polyethylene glycol 4000 from Lachema and Dowex 50 WX 8 (Serva).

3.2. Preparation and purification of phosphonic acids

According to literature [33], phosphonic acids were prepared by the Mannich type reaction of an amine, formaldehyde and phosphorous acid according to the general equation (Scheme 1.), where 37% HCl was used as a catalyst.
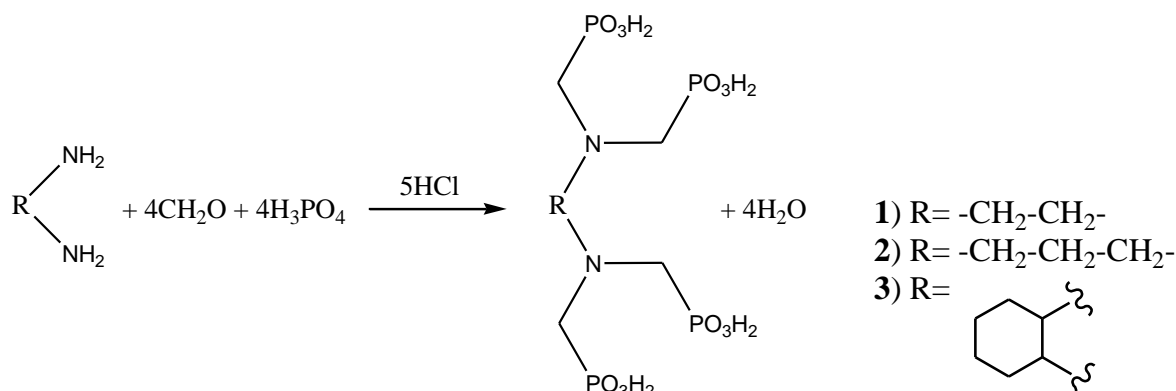
Scheme 1. Synthesis of compounds **1**, **2** and **3**.

The compounds EDTMP (**1**), PDTMP (**2**) and CDTMP (**3**) were prepared as part of research project of M. Sakmár [34].

After synthesis, the phosphonic acids were purified by the method of ion excange chromatography (Dowex 50 WX8, H$^+$ form, 200-400 mesh). Dowex ion excange resin was first washed with 1 mM HCl and then regenerated with 1 M HCl. The compound mixture was then eluted from the column using demmineralised water until pH reached a value of 4,5-6. The desired compound was eluted in the first fractions while the impurities remained on the column.

Purified phosphonic acids were fully characterized by available spectral methods (NMR, MS, FT-IR).

For mass spectra analysis, 1 mg of dried compound was dissolved in 1 mL of ultrapure water. Of that mixture, 100 µL was diluted in 1 mL of MeOH and used for analysis. To enhance the visibility of the molecular ion, 100 µL of 1% formic acid was added.

3.3.   Preparation and labelling of nanocomposites with ^{99m}Tc

Purified phosphonic acids EDTMP (**1**), PDTMP (**2**) and CDTMP (**3**), and commercially obtained methylenediphosphonic acid MDP (**4**), etidronic acid HEDP (**5**), zoledronic acid (**6**), pamidronic acid (**7**) and polyethylene glycol (**8**) were used for preparation and stabilisation of nanocomposites.

Hydroxyapatite nanoparticles were prepared by P.Mičolová and E.Kukleva as described in literature [35], by mixing 25 mL of 0,8 M $(NH_4)_2HPO_3$ and 25 mL of 1,34 M $Ca(NO_3)_2$. Before adding $Ca(NO_3)_2$, the pH value was adjusted to 9 by addition of NH_4OH. The precipitated nanoparticles were centrifuged, washed with ultrapure water and dried under reduced pressure.

Before labelling composite nanoparticles with ^{99m}Tc, a fresh solution of $SnCl_2$ was prepared by dissolving 13 mg $SnCl_2$ in 25 mL of water and 0,5 mL of the prepared $SnCl_2$ solution was added to each sample for the reduction of TcO_4^- to $^{99m}Tc^{4+}$.

A $^{99}Mo/^{99m}Tc$ generator (Fig.9) was eluted and in each elution, 5-10 mL of physiological saline (0,9% NaCl) containing TcO_4^- was obtained. Due to the decay of ^{99}Mo ($T_{1/2}$=66 h), on the first day of using the generator, the most activity (2 GBq) could be obtained, while for elution up to 4 days later, less activity was obtained (800 MBq). The saline was distributed evenly, 150-250 MBq of activity for each sample.

Figure 9. $^{99}Mo/^{99m}Tc$ generator.

3.3.1. Preparation and labelling of stabilised nanocomposites

Nanocomposites (**9-13**) were prepared by adding phosphonate ligands to 1,0 mg of prepared hydroxyapatite nanoparticles in 500 µL of ultrapure water. For stabilisation of nanoparticles, 0,01 mg of citric or 10 µL of 0,1 M hydrochloric acid was added. The samples were first dispersed in ultrasound bath for 15 min and then by sonifier for 5 min. The maximal temperature for dispersion was set to 40ºC and the amplitude was 10%. The composition of the nanocomposites is shown in **Table 3**.

Table 3. Composition of prepared samples. V(stock) is the volume of stock solution which contains 0,1 mg of phosphonate ligand.

Sample	Composite	m(HAp) [mg]	m(ligand) [mg]	c(stock) [mmolmL^{-1}]	V(stock) [µL]
9	MDP-HAp	1,0	0,1	0,014	41,9
10	CDTMP-HAp	1,0	0,1	0,015	13,3
11	HEDP-HAp	1,0	0,1	0,031	14,3
12	PDTMP-HAp	1,0	0,1	0,010	21,8
13	EDTMP-HAp	1,0	0,1	0,005	49,9

Samples **14** and **15** were prepared as shown in **Table 4**. The samples were dispersed by sonifier for 3 min at 40°C and amplitude 10%.

Table 4. Composition of nanocomposites with zoledronic and pamidronic acid.

Sample	Composite	m(HAp) [mg]	m(ligand) [mg]	c(stock) [mgmL^{-1}]	V(stock) [mL]
14	zoledronic acid-HAp	1,0	0,1	0,04	2,5
15	pamidronic acid-HAp	1,0	0,1	1,00	0,1

One, 2 and 4 mg/mL solutions of polyethylene glycol in 0,1 mL of isopropanol were prepared. Each solution was added to 1 mg of hydroxyapatite nanoparticles in 500 µL of ultrapure water (samples **16-18**, **Table 5**). The samples were dispersed for 3 min (40°C, 10%).

Table 5. Composition of nanocomposites with different concentrations of polyethylene glycol.

Sample	Composite	m(HAp) [mg]	m(PEG) [mg]	c(stock) [mgmL^{-1}]	V(stock) [mL]
16	PEG-HAp	1,0	1,0	1,0	1,0
17	PEG-HAp	1,0	2,0	2,0	1,0
18	PEG-HAp	1,0	4,0	4,0	1,0

To prepared samples (**9**-**18**), 150-250 MBq of activity was added and the activity of individual samples was measured. During incubation time of 1 h, samples were mixed on a vibratory shaker. After centrifugation at 4000 rpm for 5 min, the supernatant liquid was separated from the precipitate and its activity was measured. The precipitate was then washed 3 times with 1 mL of physiological saline and the activity of the saline was measured each time. After the last wash, to determine the labelling yield, the activity of the remaining precipitate was measured.

After the last wash, samples (**16**-**18**) were filtered through PTFE (13 mm, 0,22 µm) syringe filter and the activity of the filtrate was measured.

3.3.2. Stabilisation of nanocomposites after labelling

Samples (**9**-**13**) were prepared according to Table 3., and were not stabilised before labelling. For preparation of samples **19** and **20**, 1 mg of hydroxyapatite nanoparticles in 500 µL of ultrapure water was dispersed for 3 min at 40°C and amplitude of 10%. Unstabilised nanoparticles were labelled and the labelling yield was determined after washing the nanoparticles 3 times, as described in chapter 3.3.1.

For stabilisation of labelled nanoparticles, 0,01 mg of citric or 10 µL of 0,1 M hydrochloric (**9**-**13**); 0,1 mg of zoledronic (**19**) or pamidronic (**20**) acid was added. The samples were dispersed for 3 min at 40°C and amplitude of 10%. After dispergation, samples were filtered (PTFE 13 mm, 0,22 µm filter) and the activity of the filtrate was measured to determine the labelling yield of the complete procedure.

3.3.3. Preparation of nanocomposites after labelling

Mass of 0,1 mg of zoledronic (**21**) and pamidronic (**22**) acid was labelled with ^{99m}Tc. The samples were heated for 30 min at 70°C. The labelling yields were determined by paper chromatography on Whatman 1 paper in physiological saline and MEK [36]. 1 mg of dispersed hydroxyapatite nanoparticles in 500 µL water was added to the labelled nanoparticles and the solution was dispersed again. After 30 min, the samples were washed 3 times and measured to determine the labelling yield.

3.3.4. Stabilisation of nanocomposites during their preparation

Hydroxyapatite nanoparticles (**23**-**27**) were prepared by adding 0,07 mmol of phosphonate ligands (**1**-**7**) in 800 µL of water to 600 µL (NH$_4$)$_2$HPO$_4$. Then 600 µL of Ca(NO$_3$)$_2$ was added and the mixture was dispersed.

Nanoparticles of TiO$_2$ (**28**-**32**) were prepared by adding 800 µL of a 0,07 mmol solution of phosphonate ligands (**1**-**7**) in ultrapure water, to 2 mL of ultrapure water. To the mixture was then added 2x575 µL of TBOT:IPA. The mixture of tetra *n*-butyl orthotitanate (TBOT) and isopropyl alcohol (IPA) was prepared in a ratio of 250 µL: 900 µL. The nanoparticles were formed by the proces of hydrolysis while being dispersed by sonifier. The operating conditions of the sonifier were 3 min, maximal temperature 40°C and amplitude 30%.

Prepared nanoparticles were then washed 2 times, with water and methanol, during which they were precipitated by centrifuge at 9000 rpm. The high number of rotations per minute was used due to the small particle size.

Each sample of nanoparticles (**23**-**32**) was divided into 3 samples by taking 500 µL of dispersed nanoparticles. The samples were labelled and then washed 3 times to determine the labelling yield.

3.4.   Preparation and labelling of nanocomposites with ^{223}Ra

An ^{227}Ac/^{227}Th/^{223}Ra generator (Fig.10) was eluted using a solution of 0,7 M HNO$_3$ in 80% MeOH [37]. The eluent was evaporated on a rotary evaporator and ^{223}Ra(NO)$_2$ was

reconstituted in ultrapure water. To each sample, 2-4 µL of the solution was added so the starting activity for each sample would be approximately 7000 cps.

Figure 10. ^{227}Ac/^{227}Th/^{223}Ra generator.

3.4.1. Preparation and labelling of stabilised nanocomposites

Samples were prepared by adding 1µL (**33**, **34**) or 15 µL (**35**, **36**) of NH$_4$OH to 0,1 mg of zoledronic (**33**, **35**) and pamidronic (**34**, **36**) acid, adding the solution to 1,0 mg of hydroxyapatite and dispersing the samples (3 min, 40°C, 10%).

Approximately 2 µL of ^{223}Ra solution was added and the activity of each sample was measured. After 30 min, the samples were washed 3 times and the labelling yield was calculated.

3.4.2. Stabilisation of nanocomposites after labelling

To the 1,0 mg of hydroxyapatite nanoparticles (**37**, **38**) dispersed in 500 µL of water (3 min, 40°C, 10%), 15 µL of NH$_4$OH was added.

For labelling, 2-4 µL of ^{223}Ra was added and after 30 min of mixing, samples were washed 3 times and the remaining activity was measured. 10 µL of NH$_4$OH was added to 0,1 mg of zoledronic (**37**) and pamidronic (**38**) acid. The samples were then dispersed and after 1 h of mixing, filtered through PTFE (13 mm, 0,22 µm) filter.

4. Results and discussion

4.1.   Purification of compounds

5,14 g of CDTMP was dissolved in 25 mL H_2O and eluted through Dowex ion excange resin with 150 mL H_2O. Mass of purified compound was 5,07 g (yield=98%).

2,00 g of EDTMP was dissolved in 70 mL H_2O and eluted through Dowex ion excange resin with 100 mL H_2O. Mass of purified compound was 0,53 g (yield=26%).

0,59 g of PDTMP was dissolved in 25 mL H_2O and eluted through Dowex ion excange resin with 150 mL H_2O. Mass of purified compound was 0,25 g (yield=42%).

Figure 11. Structures of compounds **1** and **2**.

Figure 12. Compound **3**.

Spectra of purified compounds correspond to the spectra described in the literature [38].

4.2. Preparation and labelling of nanocomposites with ^{99m}Tc

Results of labelling nanocomposites with ^{99m}Tc are listed in Tables 6-15. Each sample was prepared in duplicate.

Labelling yields were calculated according to equation 2. In equations 2 and 3, A_{end} is the activity of the precipitate after washing or activity of the filtrate after filtering. A_{corr} is the value of start activity (A_{start}), corrected according to time from the begining until the end of measurments (t/ min), due to the half-life of ^{99m}Tc (T=360 min).

$$yield = \frac{A_{end}}{A_{corr}} \cdot 100 \qquad (2)$$

$$A_{corr} = A_{start} \cdot 2^{-\frac{t}{T}} \qquad (3)$$

4.2.1. Preparation and labelling of stabilised nanocomposites

Nanoparticles have a particular tendency to lower their very high surface energy, which is the origin of their thermodynamic instability. Bare nanoparticles tend to stabilise themselves either by sorption of molecules from the surroundings or by lowering the surface area through coagulation and agglomeration. In order to avoid the later, nanoparticles have to be kinetically stabilized by electrostatic, steric, or electrosteric repulsive forces [39].

Studies [10] led to the conclusion that the yield increases when the mean charge on MDP decreases so addition of citric or hydrochloric acid should increase the yields of labelling MDP as well as other phosphonate ligands because the chemical form of MDP (H_4L) in aqueous solution depends on the pH, as follows:

$$H_4L \leftrightarrow H_3L^- \leftrightarrow H_2L^{2-} \leftrightarrow HL^{3-} \leftrightarrow L^{4-} \qquad (4)$$

Decreases in pH (increases in the hydrogen ion concentration) displace the equilibrium to the left and decrease the mean charge of MDP.

To electrostatically stabilise nanocomposites of HAp and compounds **1**-**5**, citric (**Table 6**.) and hydrochloric (**Table 7**.) acid were added.
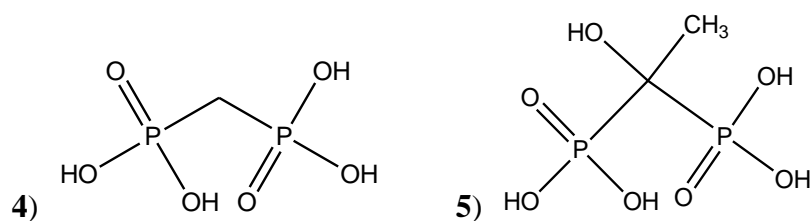
Figure 13. Methylenediphosphonic (**4**) and etidronic (**5**) acid.

Table 6. Samples **9**-**13** stabilised with citric acid. A_{start} is the activity added to each sample, A_{end} activity of precipitate after 3 washes and A_{corr} corrected value of A_{start}.

Sample	Ligand	A_{start} [MBq]	A_{end} [MBq]	A_{corr} [MBq]	Yield [%]
9	MDP	171	17	132	**13**
9	MDP	175	10	135	**7**
10	CDTMP	169	78	130	**60**
10	CDTMP	181	115	139	**83**
11	HEDP	184	14	142	**10**
11	HEDP	184	30	139	**21**
12	PDTMP	186	125	141	**88**
12	PDTMP	175	71	132	**54**
13	EDTMP	182	32	138	**23**
13	EDTMP	182	35	137	**25**

As shown in **Table 6.**, the best labelling yields are obtained with ligands CDTMP and PDTMP. The yields of other samples are very low, most of the ^{99m}Tc was not bound to the nanoparticles and was washed away.

Ligands EDTMP, PDTMP and CDTMP have two nitrogen atoms and four phosphonate groups (oxygen atoms) which are capable of coordinating to metal ions. On the

other hand, MDP and HEDP have two phosphonate groups and HEDP has one hydroxyl group. The number of coordinating atoms/groups in EDTMP, PDTMP and CDTMP is greater than that in MDP and HEDP so their complexes are more stable [40] and labelling yields for tetraphosphonates EDTMP, PDTMP and CDTMP were higher than for diphosphonates MDP and HEDP.

When the same amount of hydrochloric as citric acid was added (0,01 mg), hydroxyapatite nanoparticles were dissolved. For that reason, a smaller amount of hydrochloric acid was used (10 µL of 0,1 M HCl). Too low pH value causes dissolving of hydroxyapatite nanoparticles, or their stabilisation at a too small size.

The pH value can also effect the form of ^{99m}Tc. In a strong acidic condition, ^{99m}TcO$_4^-$ is not completely reduced. On the contrary, when the pH value is larger than 6, Na^{99m}TcO$_4$ will be easily changed into the colloid of ^{99m}Tc by SnCl$_2$ under the alkaline condition, and therefore, the yield will decrease significantly. So, the best pH value for labelling with ^{99m}Tc is 4–6 [36].

Table 7. Samples **9**-**13** stabilised with hydrochloric acid.

Sample	Ligand	A_{start} [MBq]	A_{end} [MBq]	A_{corr} [MBq]	Yield [%]
9	MDP	159	40	117	**34**
9	MDP	169	18	123	**15**
10	CDTMP	116	78	88	**89**
10	CDTMP	132	86	99	**86**
11	HEDP	164	15	120	**12**
11	HEDP	190	69	139	**50**
12	PDTMP	126	88	95	**93**
12	PDTMP	134	95	102	**93**
13	EDTMP	187	33	137	**24**
13	EDTMP	155	18	114	**16**

Results obtained when nanoparticles were stabilised with HCl were better then with citric acid. The same as with citric acid, the best yields were obtainted for CDTMP and PDTMP which confirms that tetraphosphonates make more stable complexes than diphosphonates.

Samples **14** and **15** were prepared with zoledronic and pamidronic acid (Fig.14), diphosphonates that contain one hydroxyl group, an imidazole ring (**6**) or amino group (**7**) as groups for coordinating metal ions.
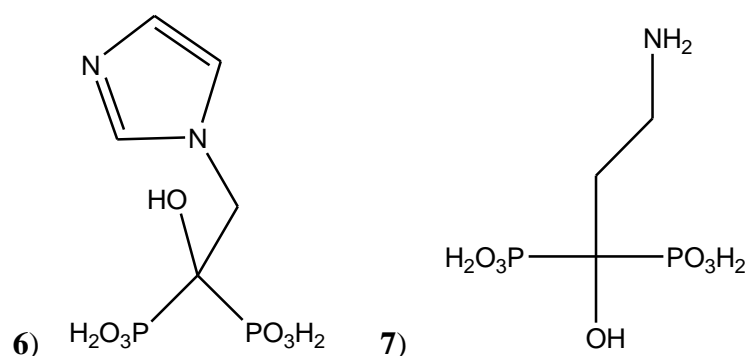
Figure 14. Structures of zoledronic (**6**) and pamidronic (**7**) acid.

Table 8. Labelling yields of samples **14** and **15**.

Sample	Ligand	A_{start} [MBq]	A_{end} [MBq]	A_{corr} [MBq]	Yield [%]
14	zoledronic acid	173	1	135	**1**
14	zoledronic acid	178	1	140	**1**
15	pamidronic acid	215	121	166	**73**
15	pamidronic acid	225	142	174	**82**

During the process of adsorption of phosphonates on HAp, charges of phosphonates and HAp change reamarkably, and the adsorption of phosphonates relaxes charges of HAp surface towards those of HAp crystal, and the HAp surface is stabilised [41].

The rapid uptake of intravenously injected particulate drug carriers by cells of the mononuclear phagocyte system (MPS) is the main limitation for drug targeting to other sites in the human body. Polyethylene glycol (PEG) polymers are at present the most popular materials to modify particulate surfaces in order to avoid recognition by cells of the MPS [42]. Nanoparticle surface properties can be modified by binding hydrophilic polyethylene glycol (PEG), which can enable them to overcome the RES capture, prolong their blood

circulation time and reduce their toxicity [3]. In literature [43], it was described that PEG is protonated in isopropanol and then adsorbed on the HAp nanoparticle surfaces, increasing their stability by an electrosteric stabilisation mechanism.
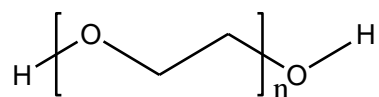
Figure 15. Polyethylene glycol (**8**).

Table 9. Stabilisation of nanoparticles with PEG.

Sample	γ(PEG) [mgL^{-1}]	A_{start} [MBq]	A_{end} [MBq]	A_{corr1} [MBq]	Yield[1] [%]	$A_{filtrate}$ [MBq]	A_{corr2} [MBq]	Yield[2] [%]
16	1	205	157	159	**98**	63	146	**43**
16	1	200	152	155	**98**	58	143	**41**
17	2	196	150	152	**99**	14	139	**10**
17	2	210	160	163	**98**	55	148	**37**
18	4	171	126	130	**97**	77	121	**63**
18	4	212	155	161	**96**	77	150	**51**

Yield after [1]Washing 3 times, [2]Filtering

Nanoparticles stabilised with PEG show good labelling yields (>96%), but due to their large size compared to the porosity of the filter (0,22 µm), approximately half of the activity remained on the filter and a fraction with a narrow size distribution was obtained.

4.2.2. Stabilisation of nanocomposites after labelling

While adding acid stabilises the nanoparticles and prevents their aggregation, it also decreses the sorption of ^{99m}Tc on the nanoparticles. To lessen the effect of acid on the sorbtion of ^{99m}Tc, acid was added to the nanoparticles after labelling.

Table 10. Samples **9-13** stabilised with citric acid after labelling.

Sample	Ligand	A_{start} [MBq]	A_{end} [MBq]	A_{corr1} [MBq]	Yield[1] [%]	$A_{filtrate}$ [MBq]	A_{corr2} [MBq]	Yield[2] [%]
9	MDP	214	103	165	**62**	69	150	**46**
9	MPD	218	79	168	**47**	56	152	**37**
10	CDTMP	218	159	168	**95**	102	150	**68**
10	CDTMP	219	160	169	**95**	108	151	**72**
11	HEDP	177	13	145	**9**	7	117	**6**
11	HEDP	172	22	141	**15**	12	114	**10**
12	PDTMP	202	153	160	**96**	82	135	**60**
12	PDTMP	199	148	157	**94**	77	131	**58**
13	EDTMP	174	38	143	**27**	17	115	**15**
13	EDTMP	180	27	148	**18**	14	119	**12**

Yield after [1]Washing 3 times, [2]Filtering

As when samples were stabilised before labelling, again samples with CDTMP (72%) and PDTMP (60%) showed the best yields. For CDTMP, HEDP and PDTMP, better yields are obtained when the nanocomposites were stabilised before labelling, while for MDP and EDTMP, yields were better when stabilised after labelling.

Table 11. Samples **9-13** stabilised with hydrochloric acid after labelling.

Sample	Ligand	A_{start} [MBq]	A_{end} [MBq]	A_{corr} [MBq]	Yield[1] [%]	$A_{filtrate}$ [MBq]	A_{corr2} [MBq]	Yield[2] [%]
9	MDP	183	48	143	**33**	32	122	**26**
9	MDP	167	41	131	**31**	25	111	**22**
10	CDTMP	164	111	128	**87**	72	108	**67**
10	CDTMP	166	111	130	**85**	39	110	**35**
11	HEDP	155	11	121	**9**	7	99	**7**
11	HEDP	150	38	117	**32**	20	96	**21**
12	PDTMP	209	155	165	**94**	90	136	**66**
12	PDTMP	198	145	156	**93**	107	130	**83**
13	EDTMP	145	42	113	**37**	23	92	**25**
13	EDTMP	165	46	129	**36**	30	105	**28**

Yield after [1]Washing 3 times, [2]Filtering

Table 12. Hydroxyapatite nanoparticles stabilised with zoledronic and pamidronic acid after labelling.

Sample	Ligand	A_{start} [MBq]	A_{end} [MBq]	A_{corr} [MBq]	Yield[1] [%]	$A_{filtrate}$ [MBq]	A_{corr2} [MBq]	Yield[2] [%]
19	zoledronic acid	214	168	177	**95**	133	168	**79**
19	zoledronic acid	242	187	200	**94**	156	190	**82**
20	pamidronic acid	223	172	173	**100**	84	158	**53**
20	pamidronic acid	235	181	181	**100**	76	166	**46**

Yield after [1]Washing 3 times, [2]Filtering

Labelled nanoparticles of HAp show very good yields >94%) but after stabilisation, the yields decresed, to 82% for zoledronic and 53% for pamidronic acid.

4.2.3. Preparation of nanocomposites after labelling

Yields of labelling zoledronic and pamidronic acid were measured by paper chromatography. When MEK was used as mobile phase, ^{99m}Tc-zoledronic acid remained at the start (R_f = 0,008) and the yield was 83%. In saline, ^{99m}Tc-zoledronic acid moved with the front (R_f = 0,969, yield=88%). In MEK, ^{99m}Tc-pamidronic acid had R_f = 0,000 and yield 100%, while in saline, the values were R_f = 0,001 and yield=100%.

The labelled acids were added to HAp and for samples with zoledronic acid, none of the added activity bound to the nanoparticles.

Table 13. Preparation of nanocomposites with labelled phosphonic acids.

Sample	Ligand	A_{start} [MBq]	A_{end} [MBq]	A_{corr} [MBq]	Yield [%]
21	zoledronic acid	243	0	154	0
21	zoledronic acid	249	0	158	0
22	pamidronic acid	177	77	122	63
22	pamidronic acid	186	65	128	51

By comparing the results of labelling before and after stabilisation with zoledronic and pamidronic acid, and preparing nanocomposites after labelling, conclusions can be made concerning the competition between HAp and phosphonates for binding of metal ions. In the case of zoledronic acid, very low yields (0-1%) were obtained when labelling stabilised nanoparticles and when nanocomposites were prepared after labelling, which could mean that zoledronic acid has higher affinity for ^{99m}Tc than HAp does so all the activity was bound by zoledronic acid and was washed away instead of remaining on the precipitate. When HAp was first labelled with ^{99m}Tc, ^{99m}Tc remained bound to HAp even after zoledronic acid was added and a higher yield was obtained. In case of pamidronic acid, the best yields were obtained when labelling after stabilisation which colud mean that the competition is not as high as with zoledronic acid.

4.2.4. Stabilisation of nanocomposites during their preparation

Phosphonate ligands were added during the preparation of nanoparticles (**23**-**32**). The highest yields were obtained for ligands MDP and HEDP. Very low yields were obtained for EDTMP, possibly due to the poor solubility of EDTMP in water.

Table 14. Hydroxyapatite nanocomposites (**23**-**27**).

Sample	Ligand	A_{start} [MBq]	A_{end} [MBq]	A_{corr} [MBq]	Yield [%]
23	MDP	61	32	37	**87**
23	MDP	37	19	21	**92**
23	MDP	60	32	35	**92**
24	CDTMP	56	19	34	**57**
24	CDTMP	53	18	29	**61**
24	CDTMP	58	24	34	**72**
25	HEDP	43	23	26	**89**
25	HEDP	62	32	34	**93**
25	HEDP	116	51	67	**76**
26	PDTMP	126	51	76	**67**
26	PDTMP	44	16	24	**65**
26	PDTMP	53	22	31	**72**
27	EDTMP	58	1	35	**2**
27	EDTMP	68	1	38	**2**
27	EDTMP	62	1	36	**4**

Labelling of TiO$_2$ nanoparticles (**Table 15**) showed very high yields, >90% for all samples. The TiO$_2$ nanoparticles were formed by process of hydrolysis with phosphonates present in the solution and the nanocomposites were formed in a way that enabled binding of all the added ^{99m}Tc, regardless of the type of phosphonate used.

Table 15. TiO$_2$ nanocomposites (**28**-**32**).

Sample	Ligand	A_{start} [MBq]	A_{end} [MBq]	A_{corr} [MBq]	Yield [%]
28	MDP	57	33	34	**98**
28	MDP	53	29	30	**97**
28	MDP	71	40	39	**101**
29	CDTMP	59	34	35	**98**
29	CDTMP	70	37	39	**95**
29	CDTMP	61	32	35	**93**
30	HEDP	44	25	26	**96**
30	HEDP	62	33	34	**96**
30	HEDP	61	33	35	**95**
31	PDTMP	55	32	32	**99**
31	PDTMP	55	31	31	**101**
31	PDTMP	59	33	33	**99**
32	EDTMP	58	34	34	**100**
32	EDTMP	56	31	31	**100**
32	EDTMP	58	33	33	**100**

4.3.   Preparation and labelling of nanocomposites with ^{223}Ra

Nanoparticles labelled with ^{223}Ra were precipitated with ligands **6** and **7**. Equation 5 was used for calculating labelling yields. A_{end} is the activity of the precipitate after washing or activity of the filtrate after filtering. The corrected value A_{corr} was caltulated according to equation 6 for labelling of stabilised nanoparticles or equation 7 for nanocomposites that were stabilised after labelling. Due to the long half-life of ^{223}Ra (11,4 days) and the short time of experiments (4 hours), A_{corr} was not corrected for the decay over time of the experiments, as with ^{99m}Tc.

$$yield = \frac{A_{end}}{A_{corr}} \cdot 100 \tag{5}$$

$$A_{corr} = A_{end} + A_s + \sum A_{wash} \tag{6}$$

$$A_{corr2} = A_{filtrate} + A_s + \sum A_{wash} + A_{filter} + A_{tube} \tag{7}$$

4.3.1. Preparation and labelling of stabilised nanocomposites

Hydroxyapatite is a good candidate for ^{223}Ra labelling, since Ra/Ca analogy allows direct radium incorporation into the structure of nanoparticles or even its re-sorption together with daughter nuclei on the NPs surface [35].

Yields obtained for labelling with ^{223}Ra are lower then for labelling with ^{99m}Tc. Due to nitric acid beeing added to the samples together with radium, pH of the solution of nanoparticles was too low which caused the nanoparticles to dissolve. To prevent nanoparticles from dissolving, more NH$_4$OH was added (Table 17.) and the labelling yields were increased.

Table 16. Labelling of samples **33** and **34** at pH=6.

Sample	Ligand	A_{start} [cps]	A_{end} [cps]	A_{corr} [cps]	Yield [%]
33	zoledronic acid	4383	1858	5137	**36**
33	zoledronic acid	6308	951	7217	**13**
34	pamidronic acid	8671	399	9030	**4**
34	pamidronic acid	7628	171	7853	**2**

Table 17. Labelling of samples **35** and **36** at pH=9.

Sample	Ligand	A_{start} [cps]	A_{end} [cps]	A_{corr} [cps]	Yield [%]
35	zoledronic acid	4416	1044	5164	**20**
35	zoledronic acid	7262	1378	8242	**17**
36	pamidronic acid	3986	2237	4528	**49**
36	pamidronic acid	7405	4646	8393	**55**

4.3.2. *Stabilisation of nanocomposites after labelling*

Table 18. Hydroxyapatite nanoparticles stabilised with phosphonic acids after labelling (**37**, **38**).

Sample	Ligand	A_{start} [cps]	A_{end} [cps]	A_{corr1} [cps]	Yield[1] [%]	A_{filtrate} [cps]	A_{corr2} [cps]	Yield[2] [%]
37	zoledronic acid	7932	5206	7758	**67**	3082	5931	**52**
37	zoledronic acid	7833	5743	7924	**72**	3817	6360	**60**
38	pamidronic acid	5600	4338	5693	**76**	1350	3344	**40**
38	pamidronic acid	9470	6517	9688	**67**	2987	7171	**42**

Yield after [1]Washing 3 times, [2]Filtering

Labelling of HAp nanoparticles with ^{223}Ra gave lower yields than with ^{99m}Tc. When nanoparticles were stabilised before labelling, ^{223}Ra-pamidronic acid-HAp showed better yields (55%) than ^{223}Ra-zoledronic acid-HAp (20%), while in case of stabilisation of nanoparticles after labelling, better results were obtained for ^{223}Ra-zoledronic acid-HAp (60%). Again as with labelling with ^{99m}Tc, there is a competition between phosphonate ligands and HAp for binding ^{223}Ra. The higher affinity of zoledronic acid for ^{223}Ra then HAp caused low yields when labelling stabilised nanoparticles.

5. Conclusions

Phosphonic acids EDTMP, PDTMP and CDTMP were purified by ion exchange chromatography.

Composite nanoparticles were prepared by precipitating EDTMP, PDTMP, CDTMP and commercially obtained MDP, HEDP, zoledronic acid, pamidronic acid and PEG with hydroxyapatite and TiO_2 nanoparticles. Prepared nanoparticles were labelled with ^{99m}Tc and ^{223}Ra.

Nanocomposites with MDP, HEDP, EDTMP, PDTMP and CDTMP were stabilised with citric and hydrochloric acid. The best results were obtained for ligands PDTMP (93%) and CDTMP (89%) stabilised with hydrochloric acid before labelling.

For the CDTMP, HEDP and PDTMP, better yields are obtained when the nanocomposites were stabilised before labelling, while for MDP and EDTMP, yields were better when stabilised after labelling.

Very low yields (0-1%) were obtained for labelling stabilised nanoparticles and when nanocomposites with zoledronic acid were prepared after labelling due to the competition between HAp and phosphonates for binding of ^{99m}Tc. In case of pamidronic acid, the best yields were obtained when labelling after stabilisation (82%).

Nanoparticles stabilised with PEG showed good labelling yields (>96%), but due to their large size, a lot of activity remained on the filter during filtering.

When phosphonates were added during the preparation of HAp nanoparticles, the highest yields were obtained for ligands MDP (92%) and HEDP (93%) and the lowest yields were obtained for EDTMP (4%). Labelling of TiO_2 nanoparticles during their preparation showed very high yields, >90% for all samples.

Labelling of HAp nanoparticles with ^{223}Ra gave lower yields than with ^{99m}Tc. When nanoparticles were stabilised before labelling, composites with pamidronic acid showed better yields (55%) than with zoledronic acid (20%), while in case of stabilisation of nanoparticles after labelling, better results were obtained for samples with zoledronic acid (60%).

6. References

1. Stewart, B.W., Wild, C. P., *World Cancer Report* IARC Nonserial Publication, 2014.
2. Ting, G., C.H. Chang, and H.E. Wang, *Cancer nanotargeted radiopharmaceuticals for tumor imaging and therapy.* Anticancer Res, 2009. **29**(10): p. 4107-18.
3. Psimadas, D., et al., *Molecular nanomedicine towards cancer: (1)(1)(1)In-labeled nanoparticles.* J Pharm Sci, 2012. **101**(7): p. 2271-80.
4. Gijs, M., et al., *Aptamers as radiopharmaceuticals for nuclear imaging and therapy.* Nucl Med Biol, 2016. **43**(4): p. 253-71.
5. Iyer, A.K., J. He, and M.M. Amiji, *Image-guided nanosystems for targeted delivery in cancer therapy.* Curr Med Chem, 2012. **19**(19): p. 3230-40.
6. Kramer-Marek, G. and J. Capala, *The role of nuclear medicine in modern therapy of cancer.* Tumour Biol, 2012. **33**(3): p. 629-40.
7. Janib SM, M.A., MacKay JA. Imaging and drug delivery using theranostic nanoparticles. Advanced drug delivery reviews. 2010;62(11):1052-1063. doi:10.1016/j.addr.2010.08.004.
8. Hamoudeh, M., et al., *Radionuclides delivery systems for nuclear imaging and radiotherapy of cancer.* Adv Drug Deliv Rev, 2008. **60**(12): p. 1329-46.
9. Qaim, S.M., *Nuclear data relevant to the production and application of diagnostic radionuclide.* Radiochimica Acta International journal for chemical aspects of nuclear science and technology, 2001. **89(223)**.
10. Petriev, V.M., E.L. Afanas'eva, and V.G. Skvortsov, *Osteotropic radiopharmaceuticals based on phosphonic acids for the treatment of bone metastases in humans (review).* Pharmaceutical Chemistry Journal, 2008. **42**(5): p. 233-240.
11. Luk, B.T., R.H. Fang, and L. Zhang, *Lipid- and polymer-based nanostructures for cancer theranostics.* Theranostics, 2012. **2**(12): p. 1117-26.
12. Hruby, M., et al., *New bioerodable thermoresponsive polymers for possible radiotherapeutic applications.* J Control Release, 2007. **119**(1): p. 25-33.
13. Schutt, W., et al., *Biocompatible magnetic polymer carriers for in vivo radionuclide delivery.* Artif Organs, 1999. **23**(1): p. 98-103.
14. Johnson, A.K., et al., *Highly hydrated poly(allylamine)/silica magnetic resin.* Journal of Nanoparticle Research, 2011. **13**(10): p. 4881-4895.
15. Couturier, O., et al., *Cancer radioimmunotherapy with alpha-emitting nuclides.* Eur J Nucl Med Mol Imaging, 2005. **32**(5): p. 601-14.
16. Mulford, D.A., D.A. Scheinberg, and J.G. Jurcic, *The promise of targeted {alpha}-particle therapy.* J Nucl Med, 2005. **46**(1): p. 199S-204S.
17. Kim, Y.S. and M.W. Brechbiel, *An overview of targeted alpha therapy.* Tumour Biol, 2012. **33**(3): p. 573-90.
18. Elgqvist J, F.S., Pouget J-P, Albertsson P. The Potential and Hurdles of Targeted Alpha Therapy – Clinical Trials and Beyond. Frontiers in Oncology. 2013;3:324. doi:10.3389/fonc.2013.00324.
19. Washiyama, K., et al., *227Th-EDTMP: A potential therapeutic agent for bone metastasis.* Nuclear Medicine and Biology, 2004. **31**(7): p. 901-908.
20. Cordier, D., et al., *Targeted Radiolabeled Compounds in Glioma Therapy.* Seminars in Nuclear Medicine, 2016. **46**(3): p. 243-249.
21. Chan, S.H., et al., *Influence of tumour size on the efficacy of targeted alpha therapy with 213Bi-[DOTA0,Tyr3]-octreotate.* EJNMMI Research, 2016. **6**(1): p. 1-10.
22. Kozempel, J., Vlk, M.: Nanoconstructs in Targeted Alpha-Therapy. Recent Patents on Nanomedicine. 2015, 4(2), 71-76.
23. Felber, M., et al., *99mTc Radiolabeling and Biological Evaluation of Nanoparticles Functionalized with a Versatile Coating Ligand.* Chemistry – A European Journal, 2015. **21**(16): p. 6090-6099.

24. Holzwarth U, B.E., Dalmiglio M, Kozempel J, Cotogno G, Gibson N. 7Be-recoil radiolabelling of industrially manufactured silica nanoparticles. Journal of Nanoparticle Research. 2014;16(9):2574. doi:10.1007/s11051-014-2574-0.

25. Guseva, L.I., *Radioisotope generators of short-lived α-emitting radionuclides promising for use in nuclear medicine.* Radiochemistry, 2014. **56**(5): p. 451-467.

26. Rojas, J.V., et al., *Synthesis and characterization of lanthanum phosphate nanoparticles as carriers for (223)Ra and (225)Ra for targeted alpha therapy.* Nucl Med Biol, 2015. **42**(7): p. 614-20.

27. Chakraborty, S., et al., *Preparation and preliminary studies on 177Lu-labeled hydroxyapatite particles for possible use in the therapy of liver cancer.* Nucl Med Biol, 2008. **35**(5): p. 589-97.

28. Chaudhari, S., T. Shaikh, and P. Pandey, *A Review on Polymer Tio2 Nanocomposites.* International Journal of Engineering Research and Application, 2013. **3**(5): p. 1386-1391.

29. Hildebrand, H., et al., *Strategies for radiolabeling of commercial TiO2 nanopowder as a tool for sensitive nanoparticle detection in complex matrices.* Journal of Nanoparticle Research, 2015. **17**(6): p. 1-12.

30. Han, Y.J., et al., *Controlled size and morphology of EDTMP-doped hydroxyapatite nanoparticles as model for 153Samarium-EDTMP doping.* J Mater Sci Mater Med, 2008. **19**(9): p. 2993-3003.

31. Ong, H.T., et al., *Exploiting the high-affinity phosphonate–hydroxyapatite nanoparticle interaction for delivery of radiation and drugs.* Journal of Nanoparticle Research, 2007. **10**(1): p. 141-150.

32. Mishra A.K., P.P., Mishra P., Chuttani K., Jain V., *Novel Targeted Delivery of Folate Conjugated Tetramethyl Phosphonate to Bone: Biodistribution Studies of Technetium-99m Labeled Folate-aminobenzyl Ethylene Diamine Tetramethyl Phosphonate (Folate-Bz-EDTMP).* Brig. S. K. Mazumdar Road, Timarpur Delhi-110054 INDIA

33. Moedritzer, K. and R.R. Irani, *The Direct Synthesis of α-Aminomethylphosphonic Acids. Mannich-Type Reactions with Orthophosphorous Acid.* The Journal of Organic Chemistry, 1966. **31**(5): p. 1603-1607.

34. Sakmár, M., *Synthesis and labelling of carries with ^{223}Ra.* 2016.

35. Kozempel, J., et al., *Prospective carriers of 223Ra for targeted alpha particle therapy.* Journal of Radioanalytical and Nuclear Chemistry, 2015. **304**(1): p. 443-447.

36. Qiu, L., et al., *99mTc-labeled butyl-substituted zoledronic acid as a novel potential SPECT imaging agent: preparation and preclinical pharmacology study.* Medicinal Chemistry Research, 2013. **22**(12): p. 6154-6162.

37. Guseva, L.I., G.S. Tikhomirova, and N.N. Dogadkin, *Anion-Exchange Separation of Radium from Alkaline-Earth Metals and Actinides in Aqueous-Methanol Solutions of HNO3. 227Ac-223Ra Generator.* Radiochemistry, 2004. **46**(1): p. 58-62.

38. Villemin, D., et al., *Green Synthesis of Poly(aminomethylenephosphonic) Acids.* Phosphorus, Sulfur, and Silicon and the Related Elements, 2010. **185**(12): p. 2511-2519.

39. Kraynov A., M.l.T.E., *Concepts for the Stabilization of Metal Nanoparticles in Ionic Liquids.* Applications of Ionic Liquids in Science and Technology, 2011. **InTech,** DOI: 10.5772/22111. .

40. Hashimoto K., M.H., *Analysis of ^{188}Re-EDTMP complexes by HPLC and ultrafiltration.* Radiochim. Acta 92, 285–290, 2004.

41. Ri, M.-H., et al., *Ab initio Investigation of Adsorption Characteristics of Bisphosphonates on Hydroxyapatite (001) Surface.* arXiv preprint arXiv:1604.07489, 2016.

42. Gref, R., et al., *'Stealth' corona-core nanoparticles surface modified by polyethylene glycol (PEG): influences of the corona (PEG chain length and surface density) and of the core composition on phagocytic uptake and plasma protein adsorption.* Colloids Surf B Biointerfaces, 2000. **18**(3-4): p. 301-313.

43. Kuche Loghmani, S., M. Farrokhi-Rad, and T. Shahrabi, *Effect of polyethylene glycol on the electrophoretic deposition of hydroxyapatite nanoparticles in isopropanol.* Ceramics International, 2013. **39**(6): p. 7043-7051.

Curriculum vitae

Natalija Pantalon Juraj was born on December 7., 1992. in North Vancouver, Canada. She attended primary school "Samobor" and high school "Antun Gustav Matoš" in Samobor. In 2011. she began to study Applied Chemistry at the Faculty of Chemical Engineering and Technology, University of Zagreb. She did her professional practice in the laboratory of Supramolecular and nucleoside chemistry at the "Ruđer Bosković" institute. In 2014. she defended her undergraduate thesis titled "Benzimidazole derivatives as potential optical pH sensors", under the mentorship of Assistant Professor, Ivana Steinberg, Ph.D. and became university bachelor of Applied Chemistry. In 2014. she started the first year of graduate program Applied Chemistry, module Specific Materials and Advanced Technologies, Faculty of Chemical Engineering and Technology. Under the mentorship of Assistant Professor, Ivana Steinberg, Ph.D. she wrote a research paper titled „Design, synthesis and immobilization of novel fluorescent 1,2,3-triazole coumarin derivatives, for use in (bio)chemical sensor materials" for which she recieved Dean's award. In 2015., she participated in Symposium of Student Chemists (Zagreb). Research for the experimental part of her master thesis „Preparation and characterisation of composite nanomaterials for radionuclide delivery" was done as part of an Erasmus+ exchange programme at the Faculty of Nuclear Sciences and Physical Engineering, Czech Technical University in Prague under supervision of Dr. Ján Kozempel.